Journal of Nanofluids
Vol. 5, pp. 826–838, 2016
(www.aspbs.com/jon)

ARTICLE

Hydromagnetic Flow and Heat Transfer of Williamson Nanofluid Over an Inclined Exponential Stretching Sheet in the Presence of Thermal Radiation and Chemical Reaction with Slip Conditions

T. Vijayalaxmi[1,2,*] and Bandari Shankar[1]

[1]Department of Mathematics, Osmania University, Hyderabad 500007, Telangana, India
[2]Department of Mathematics, M.V.S. Govt. Arts and Science College, Mahabubnagar 509001, Telangana, India

The effects of thermal radiation on the magnetohydrodynamic (MHD) flow and heat transfer of Williamson nanofluid over an inclined exponential stretching sheet with slips is studied in the present work. The surface velocity of the stretching sheet, transverse magnetic field are assumed to vary as exponential function, and chemical reaction effect is consider in the present study. Suitable transformations are made, resulting equations are solved using Keller-Box method. The velocity profile enhances with Williamson parameter. Convection parameter increases the velocity profile and reduces the temperature, concentration profiles. Increase in angle of inclination decreases the velocity. Raise in Buoyancy ratio values results in enhanced velocity and diminishes the temperature. The magnetic parameter decreases the fluid velocity. Temperature profile is increasing function and nanoparticle volume fraction is a decreasing function of N_c.

KEYWORDS: Williamson Nanofluid, Chemical Reaction, Thermal Radiation, Slip Boundary Condition, Inclined Sheet, MHD.

1. INTRODUCTION

The colloidal suspension of particles with 1 to 100 nm of base fluids are called Nanofluids. Recently, nanofluids become important in the research due to nano sized particles could enhances the coefficient of heat transfer in several times compared to the base fluid. The thermal conductivity could be enhance about 40% using of nanofluids and this makes to compatible for cooling and solidification systems. Nanoparticles plays vital role in heat transfer during solidification of the systems. Masuda[1] studied the improved heat transfer rate due to small particles size and this term is first presented by Choi.[2] Williamson fluid is a pseudoplastic fluid and belongs to Non-Newtonian fluid. Study of the boundary layer flow of pseudoplastic fluid is becoming important due to its great interest of wide range of application in industry. To explain the behavior of pseudoplastic fluid models like power law model, Carreaus model, Cross model and Ellis model, etc. are proposed. In 1929, Williamson consider the flow of pseudoplastic materials and proposed a model with equations to describe the flow of pseudoplastic fluids and it has been verified experimentally. Heat and mass transfer effects with the peristaltic flow of Williamson fluid in a vertical annulus is studied.[3] Vajravelu[4] reported the peristaltic transport of a Williamson fluid with permeable walls in asymmetric channel. Dapra et al.[5] reported the perturbation solution for a Williamson fluid which injected into a rock fracture. Alam Khan[6] studied the series of solutions using of homotopy analysis method (HAM) in four flow problems of a Williamson fluid. Nadeem group[7] performs the modelling of a two-dimensional flow analysis for Williamson fluid over a linear and exponentially stretching surface.

The study of magneto-hydrodynamic (MHD) flow of an electrically conducting fluid is of considerable interest in modern metallurgical and metal working processes. The process of fusing of metals in an electrical furnace by applying a magnetic field and the process of cooling of the first wall inside a nuclear reactor containment vessel where the hot plasma is isolated from the wall by applying a magnetic field are some examples of such fields.[8] Magnetic field plays an important role to control the momentum, concentration and heat transfer in the boundary layer flow

*Author to whom correspondence should be addressed.
Email: vijaya9966998024@rediffmail.com
Received: 16 June 2016
Accepted: 3 August 2016

 2169-432X/2016/5/826/013 doi:10.1166/jon.2016.1283

of fluids over a stretching sheet. In controlling momentum and heat transfers in the boundary layer flow of different fluids over a stretching sheet, applied magnetic field may play an important role.[9] Reports of Kumaran[10] gave the magnetic field makes the streamlines steeper which results the boundary layer thinner. Exact solution for MHD slip flow over a stretching sheet is studied by Fang.[11] The investigation of MHD slip flow, heat transfer over nonlinear permeable stretching surface through chemical reaction is analyzed by Yazdi.[12] Stagnation Point Flow and Convection in a Nanofluid Saturated Porous Medium with Convective Boundary Condition and Chemical Reaction is recently studied by Kameswaran et al.[13]

Chemical reactions are either heterogeneous or homogeneous and depend on interface or as single phase volume reactions. Chemical reaction plays vital role, and are design of chemical process equipment, formation and dispersion of fog, processing of food, and cooling towers. Flow study and chemical reaction became important in recent years. Chamkha[14] studied heat and mass transfer by steady flow of an electrically conducting fluid past a moving vertical surface in presence of first order chemical reaction. Chemical reaction effects are well studies.[15–17] The MHD effect of slip flow and heat transfer over a nonlinear permeable stretching surface with chemical reaction is reported.[18] The heat transfer studies of mixed convection effect over a nonlinear stretching surface with variable fluid properties is studied by Prasad et al.[19]

Study on the thermal conductivity of nanofluids is carried out by Jacopo Buongiorno.[20] The exercise is comprised of aqueous and nonaqueous basefluids, metal and metal oxide particles, near-spherical and elongated particles, at low and high particle concentrations. Heat transfer, influenced by thermal radiation has applications in many technological processes. Suspension of nano solid particles in classical fluids has a known method for the improvement of thermal conductivity of heat transfer fluids. Nadeem[21] analyzed the boundary layer flow of a nanofluid as it passes through a porous shrinking sheet with thermal radiation. Recently, Prasannakumara[22] studied the effects of chemical reaction and nonlinear thermal radiation on williamson nanofluid slip flow over a stretching sheet embedded in a porous medium.

Mixed convection boundary layer flow over an inclined stretching surface immersed in an incompressible visco elastic fluid is studied.[23] Report on numerical solution for mixed convection boundary layer flow of a nanofluid along an inclined plate embedded in a porous medium is given by Rana.[24] Rudraswamy and Gireesha[25] analysed the effect of inclination angle and magnetic field on flow and heat transfer of a nanofluid over an impermeable stretching sheet. Shit[26] studied on hydromagnetic flow over an inclined non-linear stretching sheet with variable viscosity in the presence of thermal radiation and chemical reaction. Recent studied on effects of magnetic field and chemical reaction on stagnation-point flow and heat transfer of a nanofluid over an inclined stretching sheet.[27]

The no-slip boundary condition is recognized as the key expression of the Navier–Stokes theory of fluid dynamics. As the situations where in such condition is not appropriate. In particular, no-slip condition is inadequate for non-Newtonian liquids and nanofluids. Some polymer melt often shows microscopic wall slip and that in general is governed by a non-linear and monotone relation between the slip velocity and the traction. Andersson[28] studied a closed form solution of a full Navier–Stokes equations for a MHD flow over a stretching sheet. Wang[29] reported the closed form similarity solution of a full Navier–Stokes equations for the flow due to a stretching sheet with partial slip. Wang[30] investigated stagnation slip flow and heat transfer on a moving plate. Nevertheless, Fang et al.[31] worked on slip MHD viscous flow over a stretching sheet analytically. Hayat[32] extended the problem of the previous researchers by incorporating thermal slip condition and discussed unsteady MHD flow and heat transfer over a permeable stretching sheet with slip condition. Hydrodynamic and thermal slip boundary layer flow over a flat plate with constant heat flux boundary condition is studied by Aziz.[33] Fang[34] found a closed form solution for viscous flow over a shrinking sheet using the second order velocity slip flow model. Flow and heat transfer over a stretching sheet by considering second order velocity slip boundary condition is analyzed.[35]

The present paper deals with the effects of thermal radiation and slip conditions on hydromagnetic flow and heat Transfer of Williamson nanofluid over an inclined exponential stretching sheet in the Presence of chemical reaction.

2. FLUID MODEL

Details of the Williamson fluid model is described by Nadeem and Hussain.[36] For the Williamson fluid model, the Cauchy stress tensor S is defined as[5]

$$S = -pI + \tau \tag{1}$$

$$\tau = \left(\mu_\infty + \frac{\mu_0 - \mu_\infty}{1 - \Gamma\gamma}\right) A_1 \tag{2}$$

where τ is the extra stress tensor, μ_0 is the limiting viscosity at zero shear rate, μ_∞ is the limiting viscosity at the infinite shear rate, $\Gamma > 0$ is a time constant, $A1$ is the first Rivlin-Erickson tensor, and γ is defined as

$$\gamma = \sqrt{\frac{1}{2}\pi}, \quad \pi = trace(A_1^2) \tag{3}$$

Here, we consider the case in which $\mu_\infty = 0$, $\Gamma\gamma > 1$.

ARTICLE

Finally, we get,

$$\tau = \frac{\mu_0}{1-\Gamma\gamma} A_1 \tag{4}$$

$$\text{or } \tau = \mu_0(1+\Gamma\gamma)A_1 \tag{5}$$

3. FORMULATION OF THE PROBLEM

Consider the steady two-dimensional MHD flow and heat transfer along with the chemical reaction phenomenon of an incompressible, viscous and electrically conducting Williamson nanofluid past over an inclined exponential stretching sheet coinciding with the plane $y = 0$. The flow is confined to $y > 0$. Two equal and opposite forces are applied along the x-axis, the wall is stretched and keep the origin as fixed (Fig. 1) with the velocity $U = U_W = U_0 e^{x/L}$. The x-axis is assumed to be in the direction of the flow and y-axis is normal to it. The temperature and the species concentration are maintained at a prescribed constant value $T = T_W(x) = T_\infty + T_0 e^{2x/L}$ and $C = C_w = C_\infty + C_0 e^{2x/L}$ at the sheet and T_∞ and C_∞ are the fixed values far away from the sheet. A uniform strong magnetic field of strength $B = B_0 e^{x/2L}$, where B_0 represents the constant magnetic field strength perpendicular to the sheet is imposed along the perpendicular to the sheet (Fig. 1). We assume that the induced magnetic field produced by the motion of an electrically conducting fluid is negligible, since there is no electric field as the negligible polarization of charges. The effect of induced magnetic field can also be neglected due to low electrical conductivity of the fluid which in turn produces low magnetic Reynolds number.

The continuity, momentum, energy and concentration equations governing such type of flow are written as[36]

$$\frac{\partial u}{\partial x} + \frac{\partial v}{\partial y} = 0 \tag{6}$$

$$u\frac{\partial u}{\partial x} + v\frac{\partial u}{\partial y} = \upsilon\frac{\partial^2 u}{\partial y^2} + \sqrt{2}\upsilon\Gamma\frac{\partial u}{\partial y}\frac{\partial^2 u}{\partial y^2} + [g\beta_T(T-T_\infty) + g\beta_C(C-C_\infty)]\cos\theta - \frac{\sigma B^2}{\rho}u \tag{7}$$

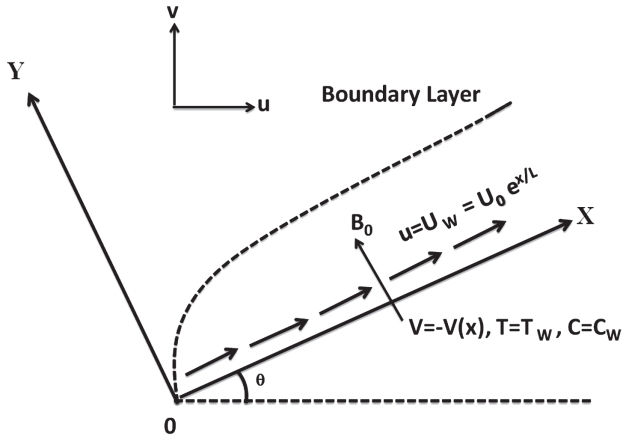

Fig. 1. Physical interpretation of the coordinate system.

$$u\frac{\partial T}{\partial x} + v\frac{\partial T}{\partial y} = \alpha\frac{\partial^2 T}{\partial y^2} + \tau\left[D_B\frac{\partial C}{\partial y}\frac{\partial T}{\partial y} + \frac{D_T}{T_\infty}\left(\frac{\partial T}{\partial y}\right)^2\right] - \frac{1}{\rho c_p}\frac{\partial q_r}{\partial y} \tag{8}$$

$$u\frac{\partial C}{\partial x} + v\frac{\partial C}{\partial y} = D_B\frac{\partial^2 C}{\partial y^2} + \frac{D_T}{D_\infty}\frac{\partial^2 T}{\partial y^2} - k_0(C - C_\infty) \tag{9}$$

The proper boundary conditions[37] for the problem is represent by

$$u = U_W + F\frac{\partial u}{\partial y}, \quad V = -V(x), \quad T = T_W(x) + D\frac{\partial T}{\partial y}, \quad C = C_W(x) + E\frac{\partial C}{\partial y} \quad \text{at } y = 0,$$
$$u \to 0,\ T \to T_\infty, C \to C_\infty \quad \text{at } y \to \infty \tag{10}$$

Where F, D and E are velocity, thermal, and concentration slip factors, u and v are the velocity components along the x and y directions respectively, μ is the coefficient of fluid viscosity, g the acceleration due to gravity, β_T the coefficient of thermal expansion, β_C the coefficient of expansion with concentration. T and C are the temperature and concentration variable respectively, D the thermal molecular diffusivity, k_0 is the reaction rate constant, Cp is the specific heat at constant pressure, k is the thermal conductivity, T_∞ and ρ_∞ are the free stream temperature and density. $\upsilon = \mu/\rho$ is the kinematic viscosity, $\alpha = k/(\rho C)_f$ is the thermal diffusivity, ρ is the fluid density, D_B is Brownian diffusion coefficient, D_T is thermophoretic diffusion coefficient, $\tau = (\rho C)_p/(\rho C)_f$ is the ratio between the effective heat capacity of the nanoparticle material and heat capacity of the fluid, $V(x) > 0$ is velocity of suction and $V(x) < 0$ is velocity blowing, $V(x) = V_0 e^{x/L}$ is a special type of velocity at the wall is considered. V_0 is the initial strength of suction.

By assuming Rosseland[38] approximation as in Cortell[39] for radiation, the radiative heat flux q_r is given by

$$q_r = -\frac{4\sigma^*}{3k^*}\frac{\partial T^4}{\partial y} \tag{11}$$

where σ^* is defined as the Stefan-Boltzman constant and K is the mean absorption coefficient. The temperature differences within the flow are so small under the consideration that T^4 may be expressed as linear function of the temperature. Expanding T^4 in a Taylor series about T_∞ and neglecting the higher order terms, we obtain

$$T^4 \cong 4T_\infty^3 T - 3T_\infty^4 \tag{12}$$

Substituting Eq. (12) in Eq. (11) the modified equations of (8) and also for a boundary layer flow over a horizontal flat plate[40]

$$q_r = \frac{-4\sigma^*}{3k^*}\frac{\partial}{\partial y}(4T_\infty^3 - 3T_\infty^4) = \frac{-16\sigma^* T_\infty^3}{3k^*}\frac{\partial T}{\partial y} \quad \text{and}$$

$$\frac{\partial q_r}{\partial y} = \frac{-16\sigma^* T_\infty^3}{3k^*}\frac{\partial^2 T}{\partial y^2}$$

$$u\frac{\partial T}{\partial x} + v\frac{\partial T}{\partial y} = \alpha\left(1+\frac{4}{3}R\right)\frac{\partial^2 T}{\partial y^2} + \tau\left[D_B\frac{\partial C}{\partial y}\frac{\partial T}{\partial y} + \frac{D_T}{T_\infty}\left(\frac{\partial T}{\partial y}\right)^2\right] \quad (13)$$

By introducing the suitable similarity transformations,[41]

$$\eta = \sqrt{\frac{U_0}{2\nu L}}e^{x/2L}y, \quad u = U_0 e^{x/L}f'(\eta),$$
$$v = -\sqrt{\frac{\nu U_0}{2L}}e^{x/2L}(f(\eta)+\eta f'(\eta)), \quad (14)$$
$$T = T_\infty + T_0 e^{2x/L}, \quad C = C_\infty + C_0 e^{2x/L}$$

and upon substitution of Eq. (14) in Eqs. (7), (13) and (9) the governing equations transforms to

$$f''' + ff'' - 2f'^2 + \lambda f'' f''' - Mf' + 2Ri(G+NH)\cos\theta = 0 \quad (15)$$

$$\left(1+\frac{4}{3}R\right)G'' + Pr(fG' - 4f'G) + \frac{N_c}{Le}G'H' + \frac{N_c}{LeN_{bt}}G'^2 = 0 \quad (16)$$

$$H'' + Sc(fH' - 4f'H) + \frac{1}{N_{bt}}G'' - \gamma H = 0 \quad (17)$$

where f, G and H are functions of η and prime denotes derivatives with respect to η; $\lambda = \Gamma(\sqrt{U_0^3 e^{3x/L}/\nu L})$ denotes the non-Newtonian Williamson parameter; $M = (2\sigma B_0^2 L)/\rho U_0$ is the magnetic parameter; $Ri = Gr_x/Re^2$ is the mixed convection parameter (Richardson number), where $Gr_x = (2g\beta_T T_0 L^3 e^{2x/L})/\nu^2$ is the Grashof number and $Re = (U_w L)/\nu$ is the Reynolds number; $N = (\beta_c C_0/\beta_T T_0)$ is the buoyancy ratio; θ the angle of inclination of the stretching sheet with the horizontal line; $R = (4\sigma^* T_\infty^3/k^*\alpha(\rho c)_p)$ is the thermal radiation; $Pr = \nu/\alpha$ is the Prandtl number denotes momentum diffusivity/nanofluid thermal diffusivity; $Sc = \nu/D_B$ represents the Schmidt number denotes momentum diffusivity/Brownian diffusivity; $N_c = \rho_p c_p/(\rho c(C_w - C_\infty))$ denotes the heat capacities ratio, which is equal to nanoparticles heat capacity/nanofluid heat capacity; $N_{bt} = (D_B T_\infty (C_W - C_\infty))/(D_T(T_W - T_\infty))$ denotes the diffusivity ratio, i.e., Brownian diffusivity/thermophoretic diffusivity; $Le = \alpha/D_B$ Lewis number denotes the nanofluid thermal diffusivity/Brownian diffusivity; $\gamma = (Sck_0)/U_0$ is a chemical reaction parameter.

The transformed boundary conditions are

$$f = S, \quad f' = 1+\alpha f'', \quad G' = 1+\beta G'',$$
$$H' = 1+\delta H'' \quad \text{at } \eta = 0 \quad (18)$$
$$f' = 0, \quad G = 0, \quad H = 0 \quad \text{as } \eta \to \infty$$

where $\alpha = F\sqrt{U_0/(2\nu L)}e^{x/(2L)}$, $\beta = D\sqrt{U_0/(2\nu L)}e^{x/(2L)}$, $\delta = E\sqrt{U_0/(2\nu L)}e^{x/(2L)}$ represent the velocity, thermal, and concentration slip parameters, $S = V_0/\sqrt{(b\nu/2L)} > 0$ (or < 0) is the suction (or blowing) parameter. If $\lambda = 0$, the problem reduces to the Newtonian nanofluid, and if $D_B = D_T = 0$, Eq. (13) reduces to a classical boundary layer heat equation in the absence of viscous dissipation. Physical quantities of interest are local skin friction coefficient C_f, local Nusselt number N_u, and local Sherwood number S_h, which are defined as

$$C_f = \frac{\tau_w}{\rho U_w^2}, \quad Nu_x = \frac{Lq_w}{k(T_w - T_\infty)}, \quad Sh_x = \frac{Lq_m}{D_B(C_w - C_\infty)}$$
$$\text{where } \tau_w = \mu_0\left(\frac{\partial u}{\partial y} + \frac{\Gamma}{\sqrt{2}}\left(\frac{\partial u}{\partial y}\right)^2\right)_{y=0},$$
$$q_w = -k\left(\frac{\partial T}{\partial y}\right)_{y=0}, \quad q_m = -D_B\left(\frac{\partial C}{\partial y}\right)_{y=0} \quad (19)$$

q_w is the heat flux at the surface, q_m is the mass flux at the surface, k is the thermal conductivity of the fluid. By substituting Eq. (14) into Eq. (19) we will get

$$\sqrt{2Re}C_f = (f''(0) + \frac{\lambda}{2}f''^2(0)),$$
$$Nu_x\sqrt{\frac{2}{Re}} = -\left(1+\frac{4}{3}R\right)G'(0), \quad Sh_x\sqrt{\frac{2}{Re}} = -H'(0) \quad (20)$$

where, $Re = (U_w L)/\nu$ local Reynolds number.

4. NUMERICAL METHOD

The ordinary differential Eqs. (15)–(17) with the boundary conditions of Eq. (18) are solved numerically by using of Keller-Box method, as revealed by Refs. [42, 43], the following few steps are involved to achieve Numerical solutions:

- Reduce the above mentioned higher order ordinary differential equations into a system of first order ordinary differential equations;
- Write the finite differences for the first order equations.
- Linearize the algebraic equations by Newton's method, and write them in matrix–vector form; and
- Solve the linear system by the block tri-diagonal elimination technique. To get the accuracy of this method the appropriate initial guesses have been chosen.

The following initial guesses are chosen.

$$f_0(\eta) = S + \left(\frac{1}{1+\alpha}\right)(1-e^{-x}), \quad G_0(\eta) = \left(\frac{1}{1+\beta}\right)e^{-x},$$
$$H_0\left(\eta\right) = \left(\frac{1}{1+\delta}\right)e^{-x}$$

The choices of the initial guesses depend on the convergence criteria and the wall shear stress $f''(0)$ is commonly used as a convergence criterion because the greatest error appears in the wall shear stress parameter in the boundary layer flow calculations as it is explained in earlier reports.[43] Thus, we used this convergence criterion in the

ARTICLE

present study. A uniform grid of size 0.004 is chosen to satisfy the convergence criterion of 10^{-7} in our study, which gives about four decimal places accurate to most of the prescribed quantities. From the process of numerical computation, the numerical values of the local Nusselt number, Skin friction coefficients and Sherwood number are represented in tabular form.

5. RESULTS AND DISCUSSION

The transformed momentum, energy and concentration equations subjected to the boundary conditions are numerically solved using the Keller-Box method. Numerical solutions are obtained and expressed in terms of graphs for a ranges of slip boundary condition and for different choices of the flow parameters. Effect of various parameters like λ, M, Ri, N, θ, α, S, R, Pr, N_c, N_{bt}, β, Le, γ, δ and Sc on velocity, temperature, and nanoparticle are studied and expressed the results in the respective graphs.

To find the correctness of the present study, a comparison have been made with the previous[22, 36, 43, 44] reports and are excellent agreements which are displayed in Table I. Moreover, the values of the skin friction coefficient, local Nusselt number and Sherwood number of different parameters are given in Tables II–IV.

Figure 2 shows the effect of magnetic parameter M on dimensionless velocity by keep the other parameters are fixed. The presence of magnetic field in an electrically conducting fluid induces the opposite force to the flow of nanofluid direction, and is called as Lorentz force, which is opposes the fluid flow. As the increased resistive force initiates to slow down the fluid flow, results to magnetic parameter decreases the velocity. As value of magnetic field parameter increase the values of skin friction coefficient increase and is given in Table II.

Figures 3(a and b) represents the variation of Williamson parameter λ on velocity and temperature profiles. It is observed that the velocity is decrease with the increase of non-Newtonian Williamson fluid parameter λ; as increase in Williamson fluid parameter λ, the fluid offers more resistance to flow which causes decrease the velocity of the flow. As a result, the temperature profile increases with the increase in the Williamson parameter and is shown in Figure 3(b). In this study, variations in both the velocity and temperature are not much affected. It enhances the skin-friction coefficient and decreases the

Table I. Comparison values of $-G'(0)$ for various values of Prandtl number for viscous.

Pr	Gorla and Sidawi (1994)	B. C. Prasannakumara (2016)	S. Nadeem and S. T. Hussain (2013)	Present study
0.2	0.1691	0.1702	0.169	0.1709
0.7	0.454	0.4544	0.454	0.4539
2	0.911	0.9113	0.911	0.9118

Table II. Computed values of skin friction coefficient $\sqrt{2Re}C_f = (f''(0) + (\lambda/2)f'^2(0))$ for various values of λ, M, Ri, N, θ, α, S.

λ	M	Ri	N	θ	α	S	$-f''(0)$
0.0	1.0	0.1	0.1	$\pi/6$	0.2	1	1.6775
0.1							1.8052
0.2							2.0017
0.3							2.4435
	0.0						1.5678
	0.1						1.6150
	0.5						1.7940
	1.0						2.0017
		0					2.1253
		0.5					1.5913
		1.0					1.1799
		1.5					0.8311
			−5				2.1513
			0				2.0046
			5				1.8672
			20				1.4969
				0			2.0013
				$\pi/6$			2.0017
				$\pi/3$			2.0029
				$\pi/2$			2.0046
					0.0		2.7272
					0.5		1.4269
					1		0.9463
					2		0.5355
						−0.2	1.2387
						0	1.3350
						0.2	1.4418
						1	2.0017

Table III. Computed values of Local Nusselt number and Sherwood number for various values of R, Pr, Le, N_c, N_{bt}, β.

R	Pr	Le	N_c	N_{bt}	β	$-G'(0)$	$-H'(0)$
0						1.2315	9.1729
0.2						1.0365	9.4531
0.5						0.8466	9.7167
1						0.6602	9.9659
	0.2					0.4293	10.2659
	2					2.5201	7.0639
	5					5.2013	1.9732
	6					6.0316	0.2994
		0.01				0.0039	11.4736
		4				1.0433	9.4708
		10				1.1244	9.3279
		20				1.1532	9.2767
			0			1.1830	9.2237
			0.5			1.1181	9.3390
			1			1.0577	9.4455
			2			0.9490	9.6347
				0.01		0.5966	−15.4599
				0.5		1.1270	9.4541
				1		1.1388	10.0316
				2		1.1448	10.3264
					0	1.3485	9.0818
					0.5	0.8999	9.5775
					1	0.6752	9.8305
					2	0.4502	10.0869

Table IV. Computed values of Local Nusselt number and Sherwood number for various values of Sc, N_{bt}, γ, δ, λ.

Sc	γ	δ	λ	$-G'(0)$	$-H'(0)$
0.5				1.1647	−1.0967
1				1.1520	−0.1773
2				1.1410	1.2470
	0			1.1244	9.3269
	0.01			1.1244	9.3279
	0.05			1.1244	9.3318
	0.1			1.1244	9.3367
		0		1.1183	11.4652
		0.5		1.1305	7.1905
		1		1.1367	5.0531
			0	1.1497	9.3632
			0.1	1.1383	9.3483
			0.2	1.1244	9.3279

wall temperature gradient, wall nanoparticle volume fraction gradient with the increase in λ. These results are presented in Tables II and IV.

Figures 4(a and b) reveals the dimensionless velocity and temperature behaviour for various values of mixed convection parameter (i.e., Richardson Number, Ri). We clearly observed as the convection parameter increases, the velocity parameter is increases and diminishes the temperature profile. Table II presents the increase in Richardson number will causes an enhancement in buoyancy which leads to enhance in skin friction, accelerate the boundary layer flow.

The effects of the concentration-to-thermal-buoyancy ratio parameter (N) on dimensionless velocity and temperature are presented in Figure 5. It is clearly observed that the increase in N the velocity profile also increases.

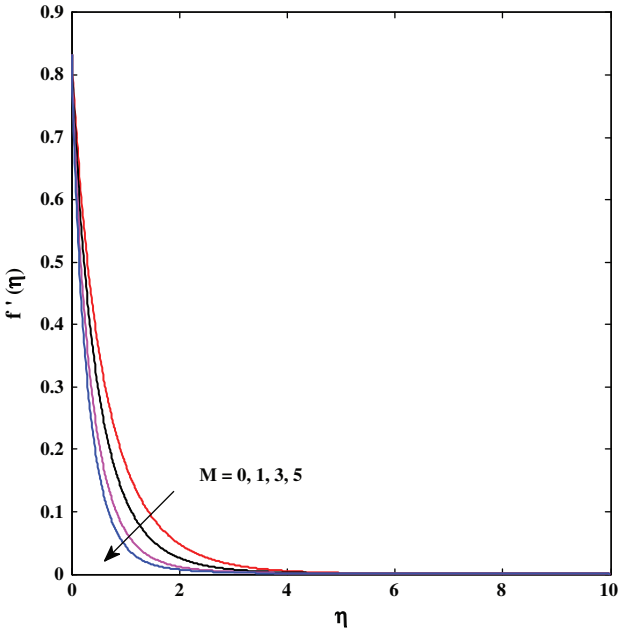

Fig. 2. Velocity variation against different values of M.

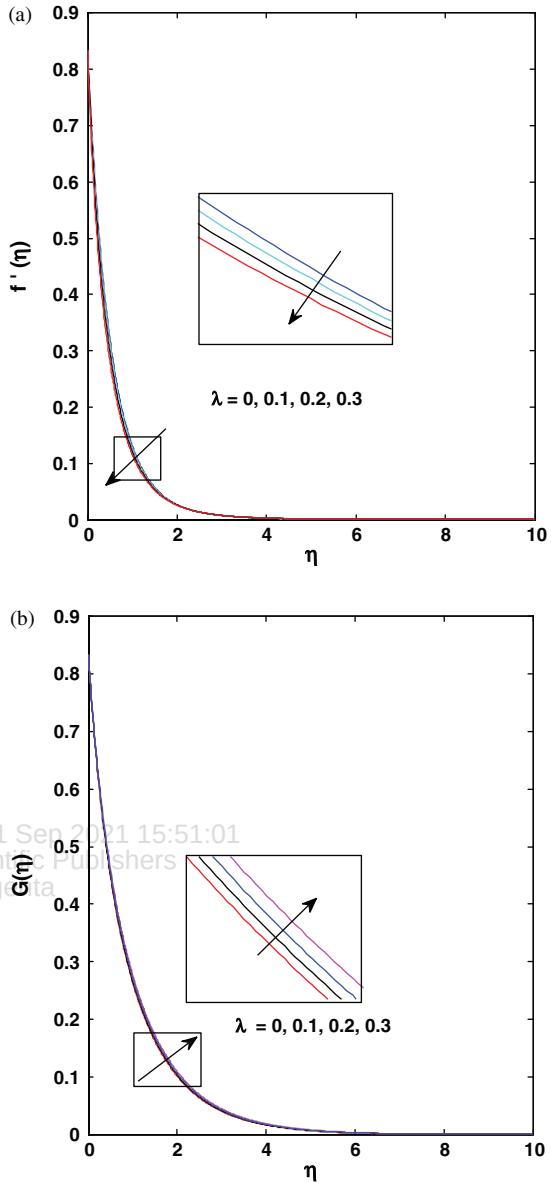

Fig. 3. Velocity and temperature variation against different values of λ.

The results are reverse in the case of temperature profile, i.e., the temperature decreases as N values are increase. Increase of N the fluid flow accelerated and its results are reflected in enhanced skin friction and is tabulated in Table II.

The effect of partial velocity slip parameter on the dimensionless velocity $f'(\eta)$ and temperature $-G(\eta)$ is depicted in Figures 6(a and b) respectively. From the Figures it is clearly observed that the velocity is decrease as increase in slip parameter. Velocity distribution is found to decrease along the boundary layer, and is reverse in the case of temperature (i.e., temperature increases with the increase in partial slip parameter). Physically, in the presence of slip, the slipping fluid shows a decrease in the surface skin-friction between the stretching sheet

ARTICLE

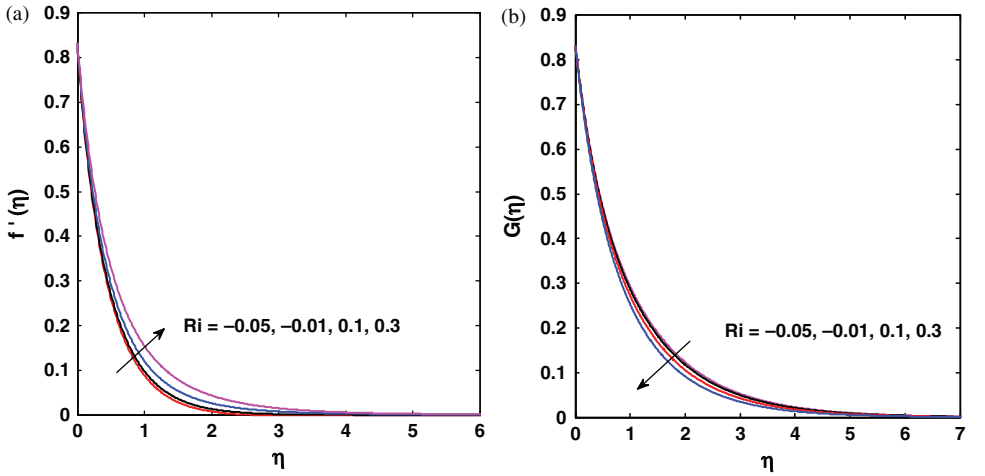

Fig. 4. Velocity and temperature variation against different values of Ri.

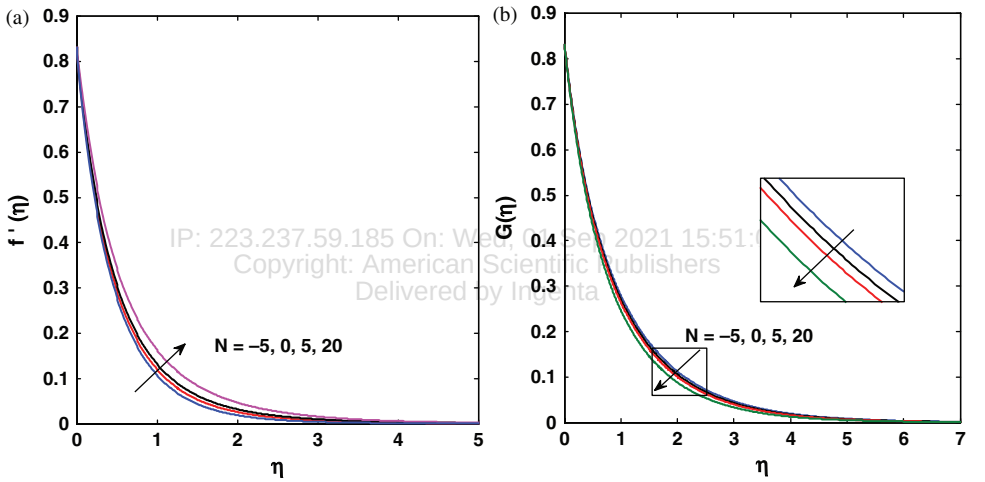

Fig. 5. Velocity and temperature variation against different values of N.

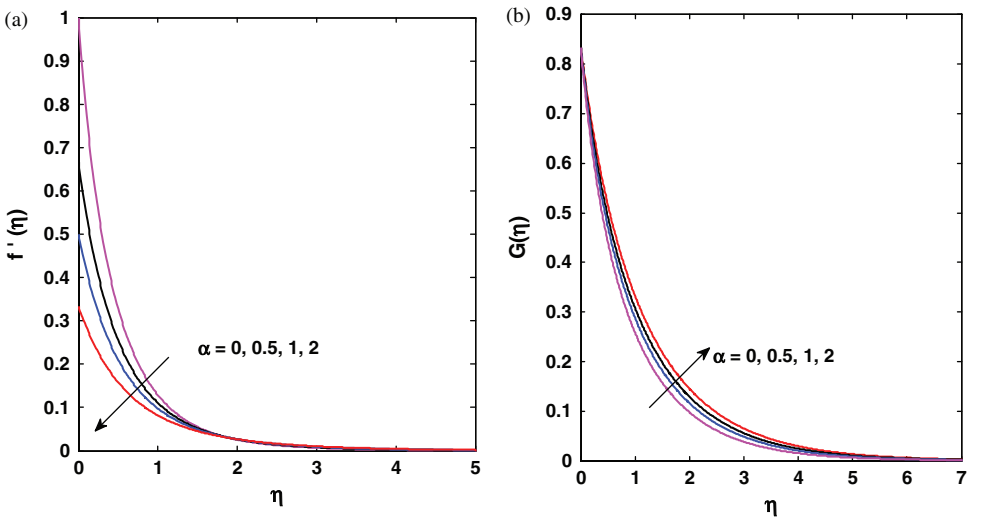

Fig. 6. Velocity and temperature variation against different values of α.

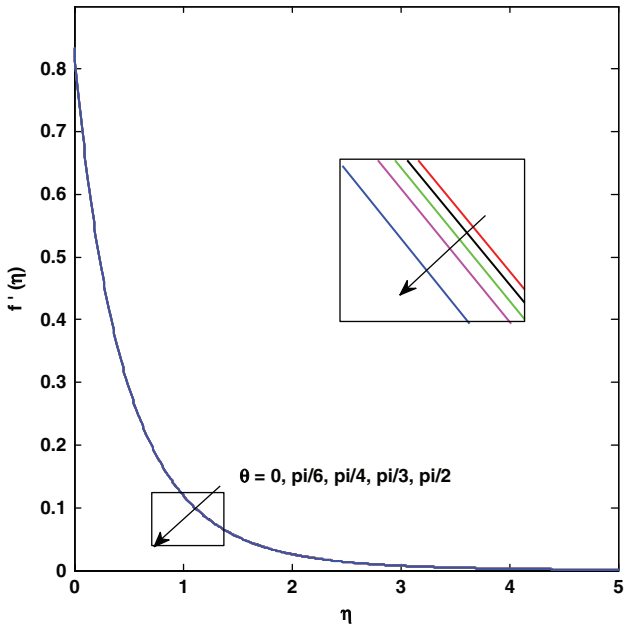

Fig. 7. Velocity and temperature variation against different values of θ.

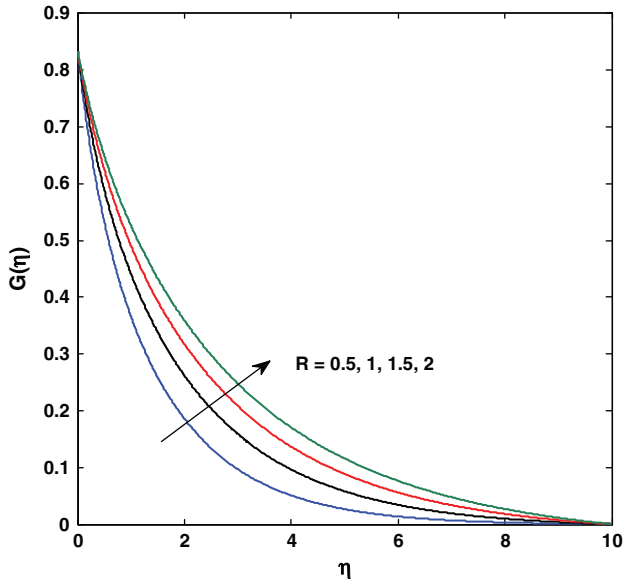

Fig. 9. Temperature variation against different values of R.

and the fluid, which is due to not all the pulling force of the stretching surface may be transferred to the fluid. Hence, the flow velocity decreases as the α increase. The increased slip parameter give the generated friction force and is allows more fluid to slip past the sheet, and the fluid flow will slows down for distances close to the sheet. The temperature parameter will enhances due to the existence of the force. Increase in momentum slip originates a reduction of penetration of the stagnant surface throughout the boundary layer, which results in momentum boundary layer thickness is increases (due to slow down flow rate with increase slip), consequently skin friction is reduces. Nevertheless, the skin friction coefficient diminishes with increase in velocity slip parameter.

The effect of angle of inclination on velocity profiles is shown in Figure 7. It clearly observed that increase in angle of inclination will decreases the velocity. Since effect of the buoyancy force depends on thermal and concentration diffusion. Henceforth, when the angle of inclination increases the effect of the buoyancy force decrease by a multiple of $\cos(\theta)$. As a result the driving force to the fluid decreases for instance a resulted velocity profiles decrease. Effect of this parameter on skin friction is almost all negligible.

The increased suction parameter S decreases the three profiles. Figure 8(a) exhibits the distinction of velocity profile with respect to the variation in suction parameter S. As the values of 'S' increase the velocity profile results in decrease. Figure 8(b) reveals the variation of temperature with suction parameter S. The increased values of suction parameter S the temperature profile decreases. Moreover, the thermal boundary layer thickness and surface temperature is also decrease. The influence of the suction parameter 'S' on the concentration profile is represented in Figure 8(c). As the values of suction parameter S increase the concentration is observed to decrease and the concentration boundary layer thickness is also decrease.

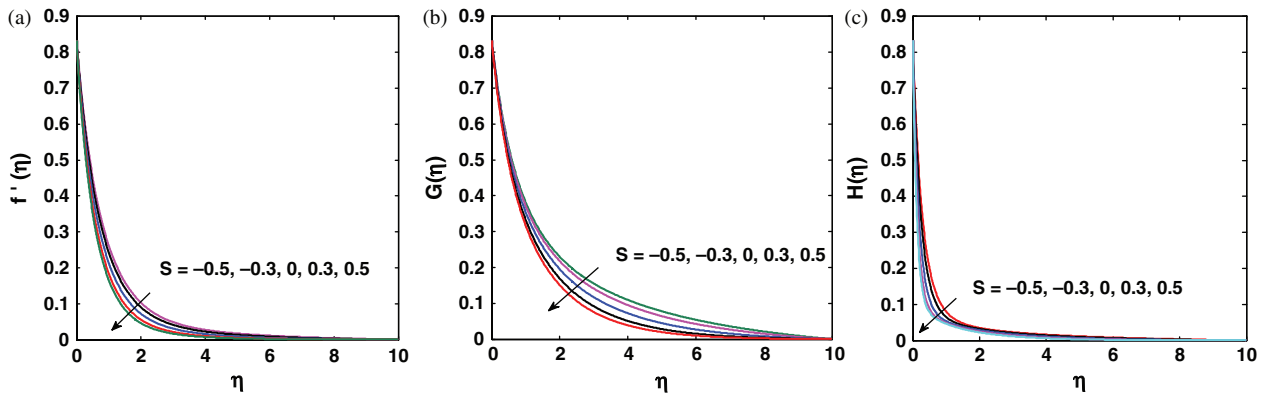

Fig. 8. Velocity, temperature and concentration variation against different values of S.

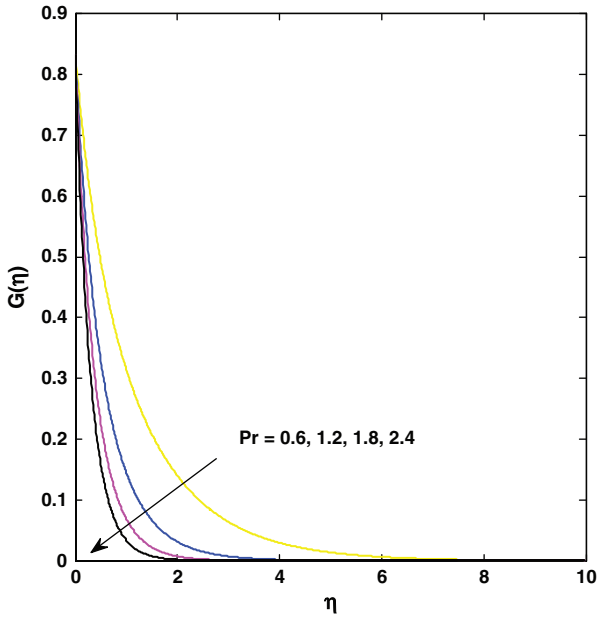

Fig. 10. Temperature variation against different values of Pr.

The value of suction parameter enhances the skin friction coefficient and is depicted in Table II.

Figure 9 demonstrates the variation of temperature with respect to radiation parameter R. When the Rosseland radiative absorptivity k^* decreases the divergence of the radiative heat flux $\partial qr/\partial y$ increases and leads to increase in rate of radiative heat transfer to the fluid at the surface (i.e., it provides more heat to the fluid which causes the fluid temperature to increase). Hence, the temperature profile as well as thermal boundary layer thickness increase as the value of thermal radiation enhances. Table III reveals the increase in the thermal radiation parameter R provides to enhance the local Sherwood number, whereas it depresses the local Nusselt number.

The effect of Prandtl number Pr on the heat transfer process is shown in Figure 10. It reveals as an increase in Prandtl number Pr the temperature field decreases. An increase in the values of Pr will reduces the thermal diffusivity, due to Prandtl number is a dimensionless number which is defined as the ratio of momentum diffusivity to thermal diffusivity ($Pr = \upsilon/\alpha$). Increase in Pr implies

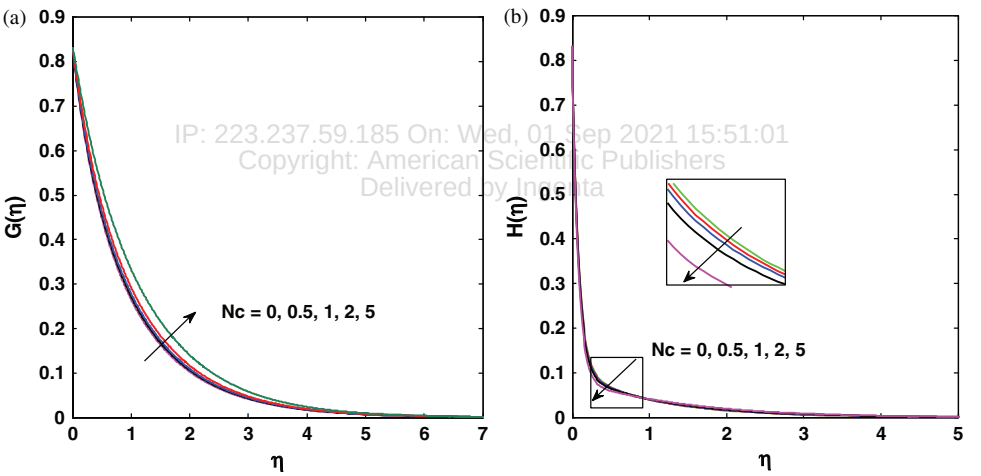

Fig. 11. Temperature and concentration variation against different values of N_c.

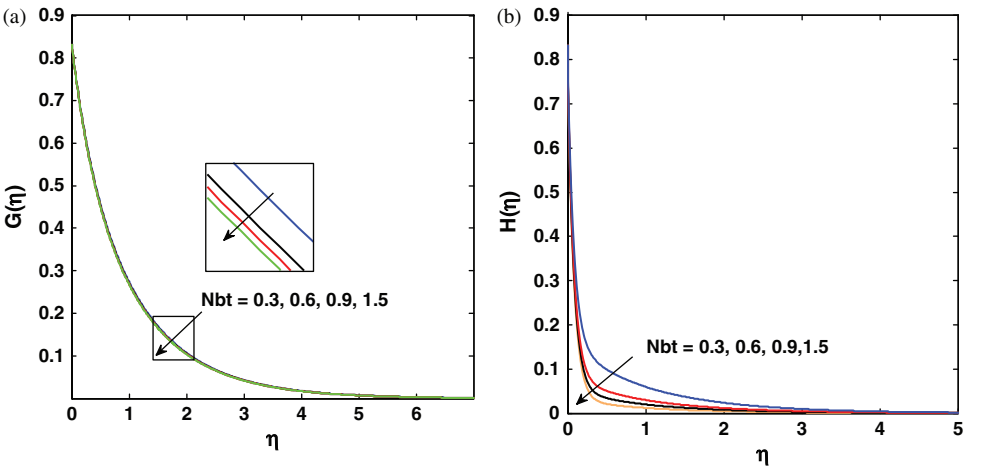

Fig. 12. Temperature and concentration variation against different values of N_{bt}.

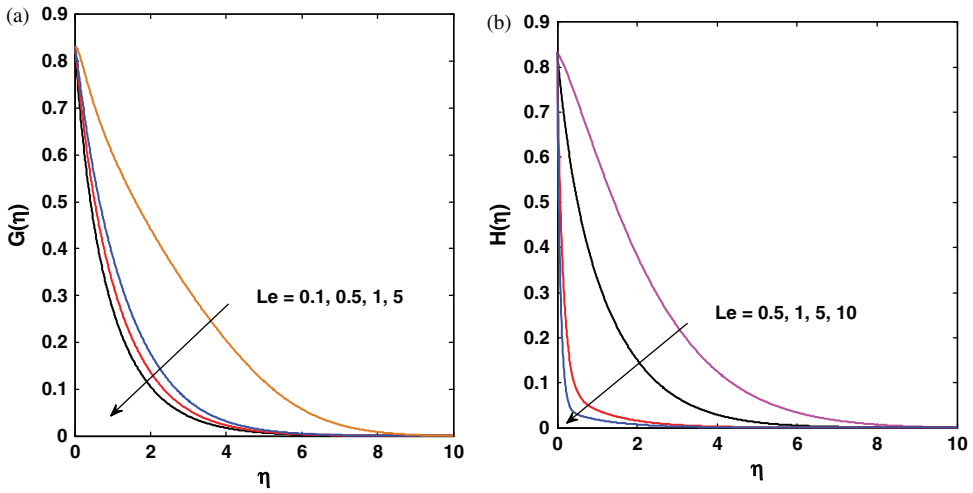

Fig. 13. Temperature and concentration variation against different values of Le.

the momentum diffusivity is higher than thermal diffusivity. Therefore thermal boundary layer thickness is a decrease function of Pr. In general, the Prandtl number is used in heat transfer problems to reduce the thickness of momentum and the thermal boundary layers. According to Table III, increase in the value of Prandtl number (Pr) leads to an increase in local Nusselt number and decrease in mass transfer rate i.e., Sherwood number.

Temperature and nanoparticle volume fraction variation against different values of N_c are depicted in Figures 11(a and b). From these graphs we can observe that the temperature profile is increasing function, whereas the nanoparticle volume fraction is a decrement function of N_c and the variation is not so much. Figures 12(a and b) show the both temperature and nanoparticle volume fraction profiles are decreases for increase in values of N_{bt}. It is observed from Table IV that the Nusselt number decreases and Sherwood number slightly increases with the increase in N_c. N_{bt} is an important heat transfer parameters for nanofluids; it is observed that the heat and mass transfer rates increases with the increase in N_{bt}.

Figure 13(b) shows the impact of Lewis number Le on concentration profile. Actually, a higher value of Lewis number $Le = \alpha/D_B$ represents a lower nanoparticle diffusivity (Brownian motion) and a higher thermal diffusivity. If $Le > 1$ the thermal diffusion rate exceeds the Brownian diffusion rate. Lower Brownian diffusion leads to less mass transfer rate as it results in the nanoparticle volume fraction (concentration) graph and the concentration

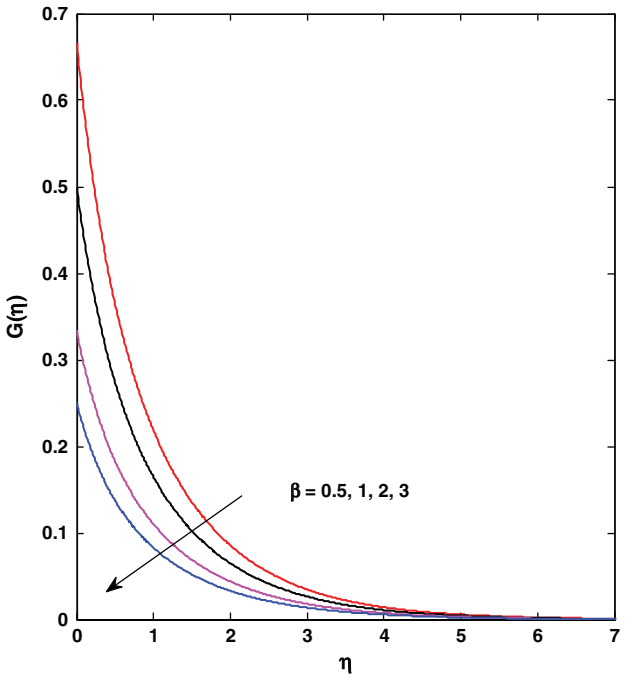

Fig. 14. Temperature variation against different values of β.

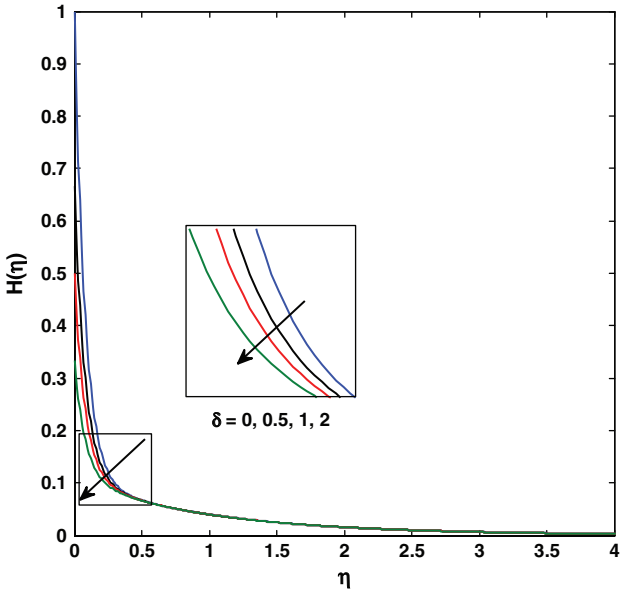

Fig. 15. Concentration variation against different values of δ.

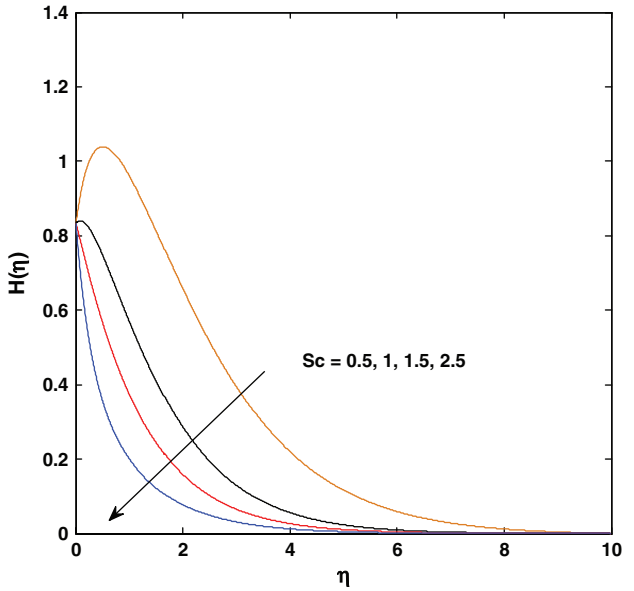

Fig. 16. Concentration variation against different values of *Sc*.

boundary layer thickness will be decrease. We can also note from Figure 13(a) the temperature and thermal boundary layer thickness decrease as increase of Lewis number *Le*. Table IV represents the variation of heat transfer rate and mass transfer rate for different values of the parameter *Le*. As the increase of Lewis number *Le* the wall nanoparticle volume fraction gradient will decreases. *Le* is also an important heat transfer parameter for nanofluids, it is observed that the heat transfer increases with the increase in *Le*.

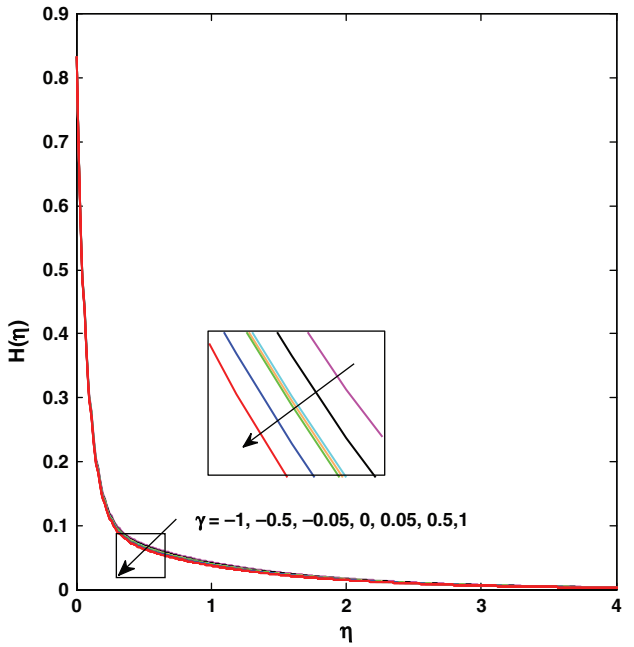

Fig. 17. Concentration variation against different values of γ.

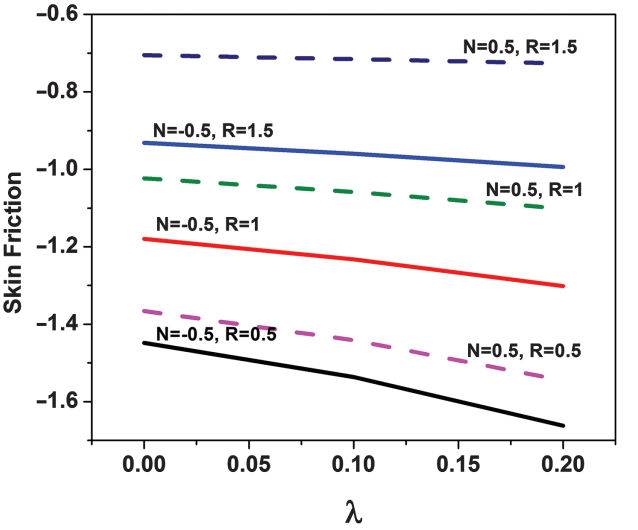

Fig. 18. Effect of λ on skin friction coefficient number against different values of N, R.

Figure 14 depicts the effect of the temperature slip boundary condition parameter β on the temperature profile. We can observe as the increase of β the temperature profile is decreased. In addition, as increases in temperature slip parameter the thermal boundary layer thickness is decreased. Because of less heat is transferred from the sheet to the fluid when the temperature slip parameter increases in magnitude. Hence, the thermal boundary layer thickness is thinner; consequently, the temperature is decreased. We can observe similar fashion from Figure 15 in the case of concentration slip parameter for concentration profile. Increase concentration slip parameter δ gives the decrease concentration. Table IV elucidates the variation of the local Nusselt number and local Sherwood number with thermal and concentration slip parameters by fixing other governing parameters.

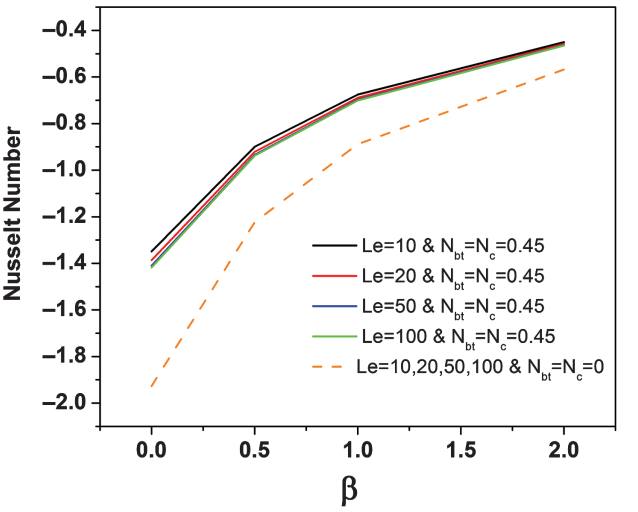

Fig. 19. Effect of β on Nusselt number against different values of Le, N_{bt}, N_c.

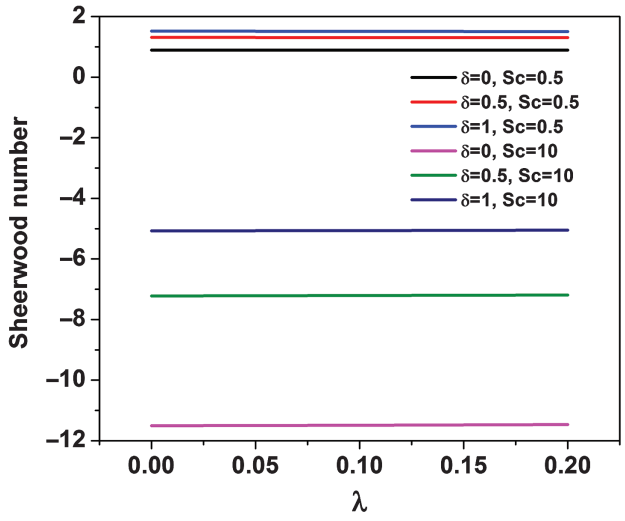

Fig. 20. Effect of λ on Sheerwood number against different values of δ, Sc.

As the increased values of thermal slip parameter β the local Nusselt number $-G'(0)$ is decreases, however, the local Sherwood number $-H'(0)$ increases and the opposite behaviour is observed for increased values of concentration slip parameter δ.

The effect of Schmidt number Sc on the mass transfer process is shown in Figure 16. This figure reveals as increase in Schmidt number Sc the concentration field is found to be decreases. An increase in the values of Sc will reduces the mass diffusivity, due to Schmidt number is a dimensionless number which is defined as the ratio of momentum diffusivity to mass diffusivity, that is $Sc = \upsilon/D_B$. Increase in Sc implies the momentum diffusivity is higher than mass diffusivity. Since, it physically relates the relative thickness of the hydrodynamic boundary layer and mass transfer (concentration) boundary layer. Therefore, the concentration boundary layer thickness is a decreasing function of Sc. From Table IV, the thermal diffusion rate decreases and conversely mass transfer will be increases in the system with increase of Sc values.

Effect of chemical reaction parameter γ on nanoparticle volume fraction profile is shown in Figure 17 for negative and positive values of γ. It is clearly observed that the nanoparticle volume fraction is decreases for constructive chemical reaction parameter and increases for destructive chemical reaction parameter. From Table IV, the chemical reaction parameter will not effect the heat transfer rate (Nusselts number), and is slightly increases the Local Sherwood number when it increases. Figures 18–20 are shows the effects of some parameters on Skin friction, Nusselts number and Sherwood number.

6. CONCLUSIONS

In the present study, we have investigated the hydromagnetic flow and heat transfer of Williamson nanofluid over an inclined exponential stretching sheet in the presence of thermal radiation and chemical reaction with slip conditions by employing a finite difference technique known as Kellor-Box method. The important findings are concluded as follows.

- The velocity decreases and temperature profile increases with increase in non-Newtonian Williamson fluid parameter λ whereas the Skin friction coefficient is increased in the presence of slip parameters.
- With the increase the values of Richardson number (mixed convection parameter) the velocity profile is increases and the temperature, concentration profiles are reduces.
- During the Buoyancy ratio parameter (N) increase, the velocity profile is enhanced and the temperature profile is decreased.
- The velocity slip parameter reduces the thickness of the momentum boundary layer, where as temperature increases with it.
- Increase in angle of inclination decreases the velocity.
- The suction parameter S decreases the three profiles when it increases.
- The temperature profile as well as thermal boundary layer thickness increases as the value of thermal radiation increases.
- Nanoparticle volume fraction decreases for constructive chemical reaction parameter and increases for destructive chemical reaction parameter.
- Solutal slip parameter significantly increases the nanoparticle volume fraction profiles.
- Temperature profile is decrease with increase in thermal slip parameter. When increase in the solutal slip parameter δ, the concentration is found to decrease.
- Increase of Prandtl number Pr results in decrease in the temperature field.
- Nanoparticle volume fraction, concentration boundary layer thickness, temperature and thermal boundary layer thickness are decreased as increase of Lewis number Le.
- Increase in Schmidt number Sc will decreases the concentration field.
- Temperature profile is increasing function, whereas nanoparticle volume fraction is a decreasing function of N_c. Both temperature and nanoparticle volume fraction profiles decrease for increase in values of N_{bt}.
- The thermal boundary layer thickness decreases with the effect of Prandtl number, and opposite behaviour is observed with the radiation parameter.

Acknowledgments: The author T. Vijayalaxmi grateful to University Grants Commission (UGC), India for awarding Faculty Development Program (FDP) and also thankful to CCE, Government of Telangana State and Principal, M.V.S. Government Arts and Science College, Mahabubnagar, Telangana State.

ARTICLE

References and Notes

1. H. Masuda, A. Ebata, and K. Teramae, *Netsu Bussei* 7, 227 (**1993**).
2. O. D. Makinde, A. Omar, and M. S. Tshehla, *Int. J. Comp. Math.* 2014, 631749 (**2014**).
3. S. Nadeem and N. S. Akbar, *Meccanica* 47, 141 (**2012**).
4. K. Vajravelu, S. Sreenadh, K. Rajanikanth, and C. Lee, *Nonlinear Anal. Real World Appl.* 13, 2804 (**2012**).
5. I. Dapra and G. Scarpi, *Int. J. Rock Mech. Mini. Sci*. 44, 271 (**2007**).
6. N. Alam Khan and H. Khan, *Nonlinear Eng*. 3, 107 (**2014**).
7. S. Nadeem, S. T. Hussain, and C. Lee, *Braz. J. Chem. Eng*. 30, 619 (**2013**).
8. W. Ibrahim, B. Shankar, and M. M. Nandeppanavar, *Int. J. Heat Mass Transfer* 56, 1 (**2013**).
9. M. Turkyilmazoglu, *Chem. Eng. Sci*. 84, 182 (**2012**).
10. V. Kumaran, A. K. Banerjee, A. Vanav Kumar, and K. Vajravelu, *Appl. Math. Comp*. 210, 26 (**2009**).
11. T. Fang, J. Zhang, and S. Yao, *Comm. Nonlinear Sci. Num. Simul*. 14, 3731 (**2009**).
12. M. H. Yazdi, S. Abdullah, I. Hashim, and K. Sopian, *Int. J. Heat Mass Transfer* 54, 3214 (**2011**).
13. P. K. Kameswaran, A. Sutradhar, P. V. S. N. Murthy, and P. Sibanda, *J. Nanofluids*. 5, 310 (**2016**).
14. A. J. Chamkha, *Int. Comm. Heat Mass Transfer*. 30, 413 (**2003**).
15. R. A. Damseh, M. Q. Al-Oda, and A. J. Chamkha, *Int. J. Therm. Sci.* 48, 1658 (**2009**).
16. E. Magyari and A. J. Chamkha, *Int. J. Therm. Sci*. 49, 1821 (**2010**).
17. K. Das, *Int. J. Heat Mass Transfer.* 54, 3505 (**2011**).
18. M. H. Yazdi, S. Abdullah, and I. Hashim, *Int. J. Heat Mass Transfer*. 54, 3214 (**2011**).
19. K. V. Prasad, K. Vajravelu, and P. S. Datti, *Int. J. Non-Linear Mech.* 45, 320 (**2010**).
20. J. Buongiorno, David C. Venerus, Naveen Prabhat, T. McKrell, J. Townsend, R. Christianson, Y. V. Tolmachev, P. Keblinski, L.-W. Hu, J. L. Alvarado, I. C. Bang, S. W. Bishnoi, M. Bonetti, F. Botz, A. Cecere, Y. Chang, G. Chen, H. Chen, S. J. Chung, M. K. Chyu, Sarit K. Das, R. D. Paola, Y. Ding, F. Dubois, G. Dzido, J. Eapen, W. Escher, D. Funfschilling, Q. Galand, J. Gao, P. E. Gharagozloo, K. E. Goodson, J. G. Gutierrez, H. Hong, M. Horton, K. S. Hwang, C. S. Iorio, S. P. Jang, A. B. Jarzebski, Y. Jiang, L. Jin, S. Kabelac, Aravind Kamath, M. A. Kedzierski, L. G. Kieng, C. Kim, J.-H. Kim, S. Kim, S. H. Lee, K. C. Leong, I. Manna, B. Michel, R. Ni, H. E. Patel, J. Philip, D. Poulikakos, C. Reynaud, R. Savino, P. K. Singh, P. Song, Thirumalachari Sundararajan, E. Timofeeva, T. Tritcak, A. N. Turanov, Stefan Van Vaerenbergh, D. Wen, S. Witharana, C. Yang, W.-H. Yeh, X.-Z. Zhao, and S.-Q. Zhou, *J. Appl. Phys.* 106, 094312 (**2009**).
21. S. Nadeem and R. U. Haq, *J. Aerosp. Eng.* 28, 04014061 (**2015**).
22. B. C. Prasannakumara, B. J. Gireesha, Rama S. R. Gorla, and M. R. Krishnamurthy, *J. Aerosp. Eng*. 29, 04016019 (**2016**).
23. G. K. Ramesh, A. J. Chamkha, and B. J. Gireesha, *Can. J. Phys.* 91, 1074 (**2013**).
24. P. Rana, R. Bhargava, and O. A. Bég, *Comp. Maths. Appl.* 64, 2816 (**2012**).
25. N. G. Rudraswamy and J. Gireesha, *J. Nanofluids* 3, 181 (**2014**).
26. G. C. Shit and S. Majee, *J. Appl. Fluid Mech.* 7, 239 (**2014**).
27. N. G. Rudraswamy, B. J. Gireesha, and A. J. Chamkha, *J. Nanofluids* 4, 1 (**2015**).
28. H. Andersson, *Acta Mech*. 158, 121 (**2002**).
29. C. Y. Wang, *Chem. Eng. Sci*. 57, 3745 (**2002**).
30. C. Y. Wang, *Chem. Eng. Sci*. 61, 7668 (**2006**).
31. T. Fang, J. Zhang, and S. Yao, *Comm. Non-Linear Sci. Num. Sim*. 14, 3731 (**2009**).
32. T. Hayat, M. Qasim, and S. Mesloub, *Int. J. Numer. Meth. Fluid* 66, 963 (**2011**).
33. I. Aziz, *Comm. Non-Linear Sci. Num. Sim*. 15, 573 (**2010**).
34. T. Fang, S. Yao, J. Zhang, and A. Aziz, *Comm. Non-Linear Sci. Num. Sim.* 15, 1831 (**2010**).
35. M. Mahantesh, K. Vajravelu, M. S. Abel, and M. N. Siddalingappa, *Int. J. Therm. Sci*. 58, 142 (**2012**).
36. S. Nadeem and S. T. Hussain, *Appl. Nanosci*. 4, 1005 (**2013**).
37. W. Ibrahim and B. Shanker, *Comp. Fluids* 75, 1 (**2013**).
38. S. Rosseland, Astrophysik und Atom-Theoretische Grundlagen, Springer, Berlin (**1931**).
39. R. Cortell, *Phys. Lett. A* 372, 631 (**2008**).
40. I. Pantokratoras and T. Fang, *Phys. Scr*. 87, 015703 (**2013**).
41. E. Magyari and B. Keller, *J. Phys. D: Appl. Phys*. 31, 577 (**1991**).
42. H. B. Keller, A New Difference Scheme For Parabolic Problems: Numerical Solution of Partial-Differential Equations. Academic, New York (**1970**).
43. T. Cebeci and P. Bradshaw, Physical and Computational Aspects of Convective Heat Transfer, Springer, New York, USA (**1988**).
44. M. Gorla and I. Sidawi, *Appl. Sci. Res*. 52, 247 (**1994**).